Contact resistance improvement using interfacial silver nanoparticles in amorphous indium-zinc-oxide thin film transistors

Rui Xu,[1,2,a)] Jian He,[1,2,a)] Yang Song,[3] Wei Li,[2] A. Zaslavsky,[1,3] and D. C. Paine[1,b)]
[1]*School of Engineering, Brown University, Providence, Rhode Island 02912, USA*
[2]*State Key Laboratory of Electronic Thin Films and Integrated Devices, University of Electronic Science and Technology of China (UESTC), Chengdu 610054, People's Republic of China*
[3]*Department of Physics, Brown University, Providence, Rhode Island 02912, USA*

(Received 8 August 2014; accepted 25 August 2014; published online 4 September 2014)

We describe an approach to reduce the contact resistance at compositional conducting/semiconducting indium-zinc-oxide (IZO) homojunctions used for contacts in thin film transistors (TFTs). By introducing silver nanoparticles (Ag NPs) at the homojunction interface between the conducting IZO electrodes and the amorphous IZO channel, we reduce the specific contact resistance, obtained by transmission line model measurements, down to $\sim 10^{-2}\,\Omega\,\mathrm{cm}^2$, $\sim$3 orders of magnitude lower than either NP-free homojunction contacts or solid Ag metal contacts. The resulting back-gated TFTs with Ag NP contacts exhibit good field effect mobility of $\sim 27\,\mathrm{cm}^2/\mathrm{V\,s}$ and an on/off ratio $>10^7$. We attribute the improved contact resistance to electric field concentration by the Ag NPs. © *2014 AIP Publishing LLC*. [http://dx.doi.org/10.1063/1.4894769]

Amorphous oxide semiconductors (AOS) based on the oxides of In, Zn, Ga, and Sn metals have found application as channel materials in thin film transistors (TFTs) used in flexible electronics and for next generation displays. Among the AOS materials, amorphous In_2O_3–10 wt. % ZnO (a-IZO) is a particularly attractive candidate material due to its high electron mobility ($\sim$15–50 $\mathrm{cm}^2/\mathrm{V\cdot s}$),[1–5] room temperature processing, amorphous structure stability,[6] and isotropic etch characteristics. In addition, the electrical resistivity can be independently tuned from $1 \times 10^{-4}\,\Omega\,\mathrm{cm}$ to $2 \times 10^{1}\,\Omega\,\mathrm{cm}$ by controlling the oxygen content in the sputter gas during deposition.[7] For TFT applications, a-IZO channel material requires low carrier density, high electron mobility, and good Ohmic contact to the source/drain electrodes. A significant challenge to AOS technology is the identification of source/drain metals with minimum specific contact resistance (ρ_C)—the resistance presented to uniform current flow across an interface of unit area between the metallization and semiconducting layers. We have reported[8] that the contact resistance of both Ti and conducting IZO channel contacts in functioning a-IZO TFTs is large ($\rho_C > 100\,\Omega\,\mathrm{cm}^2$) and is modulated by the application of gate voltage. One consequence of high contact resistance is the reduction of on-state current, which determines device performance figures of merit, including on/off ratio and switching speeds. Therefore, strategies to reduce contact resistance to a-IZO are critical to the realization of high performance a-IZO channel-based devices.

It has been suggested[9,10] that thin films embedded with nano-scale wires and particles have strikingly different properties from that of pure thin films due to the size effect. For instance, TFTs with Ag NPs embedded in the ZnO/SiO_2 interface exhibit a large clockwise hysteresis (I_D-V_G)[11] and a-SiN_x:O thin films with Ag NPs inserted between the a-SiN_x:O and Si produce highly efficient blue light emission.[12] The introduction of nanoparticles at a high specific resistance metal/semiconductor interface increases surface area and locally enhances the electric fields, thereby reducing contact resistance. Nanoparticles of Ag were chosen for this work because Ag is thermodynamically stable on IZO[13] and because procedures for fabricating uniform NPs from blanket deposits of Ag have been demonstrated[12] at relatively low temperature (300 °C).

In this work, we explored the effect of interfacial Ag NPs on the specific contact resistance of conducting/semiconducting a-IZO homojunctions and demonstrate that a reduction in contact resistance yields improved TFT device performance. Integrated TFT/TLM-patterned a-IZO structures were fabricated without Ag and with Ag NPs at the interface. The Ag nanoparticle structure is presented schematically in Fig. 1. In this structure, six identical $400 \times 2000\,\mu\mathrm{m}$ electrodes are spaced at 5 different separations d ranging from 200 μm to 1000 μm in 200 μm steps. Each electrode pair also serves as a TFT whose output and transfer characteristics were measured using an Agilent 4155 C semiconductor parameter analyzer in a light-tight probe station.

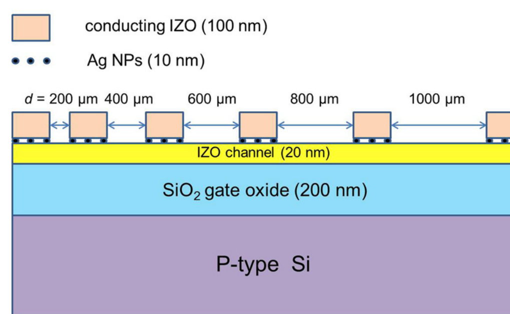

FIG. 1. Schematic view of the integrated TLM-patterned a-IZO TFTs with Ag nanoparticles at the homojunction interface between semiconducting a-IZO channel material and conducting a-IZO source-drain electrodes.

a)Rui Xu and Jian He contributed equally to this work.
b)Author to whom correspondence should be addressed. Electronic mail: David_Paine@brown.edu

 © 2014 AIP Publishing LLC

The TLM structures were fabricated on highly doped *p*-type ⟨100⟩ Si (0.001–0.005 Ω cm) substrates with thermally grown 200 nm thick SiO_2. The SiO_2 and highly doped Si were used as TFT gate dielectric and backgate metal, respectively. A 20 nm thick blanket channel layer of a-IZO (carrier concentration $\sim 10^{17}\,cm^{-3}$) was deposited at room temperature by magnetron sputtering in a reactor with 10 cm target-substrate separation (dc power density of 0.22 W/cm^2 at 280 V) in 2 mTorr of Ar/O_2 gas mixture (86:14 volume fraction). The deposition rate was ~2 nm/min. Then, a thin 10 nm Ag film was deposited through a shadow mask by electron beam evaporation in a vacuum of 5×10^{-6} Torr at room temperature. Thermal annealing was performed at 300 °C for 20 min in N_2 atmosphere to obtain roughly spherical Ag nanoparticles.[12] The Ag particles were then buried at the interface by room temperature sputter deposition of 100 nm of conducting IZO (same sputtering parameters, but in pure Ar gas, yielding a carrier concentration $\sim 10^{20}\,cm^{-3}$). For performance comparison, identical IZO TFT devices were fabricated (i) without any Ag NP interfacial layer and (ii) with 100 nm thick Ag contact metal. All of the fabricated structures were given a final air anneal at 300 °C for 1 h to ensure a similar final carrier density in the channel.

The distribution, size, and shape of Ag NPs were determined by using scanning electron microscope (SEM) and high-resolution transmission electron microscopy (HRTEM). The deposition of 10 nm Ag followed by 300 °C annealing results in the formation of discrete Ag NP spheroids as shown in the SEM plan-view (Fig. 2(a)) and with particle size in the 5–100 nm range distributed as shown in Fig. 2(b). A second conducting a-IZO layer was then deposited, embedding the NPs at the interface. Cross-sectional TEM shows that the Ag particles are hemispherical caps (Fig. 3(a)) and retain their crystalline structure (Fig. 3(b)) after all processing steps were completed.

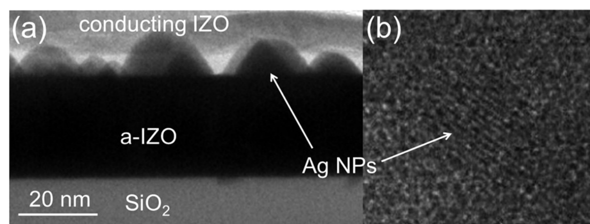

FIG. 3. (a) Cross-sectional high-resolution TEM image of conducting-IZO/Ag NP layer/semiconducting-IZO structure, the Ag particles appear as hemispherical caps; (b) single-crystal structure of the Ag nanoparticle.

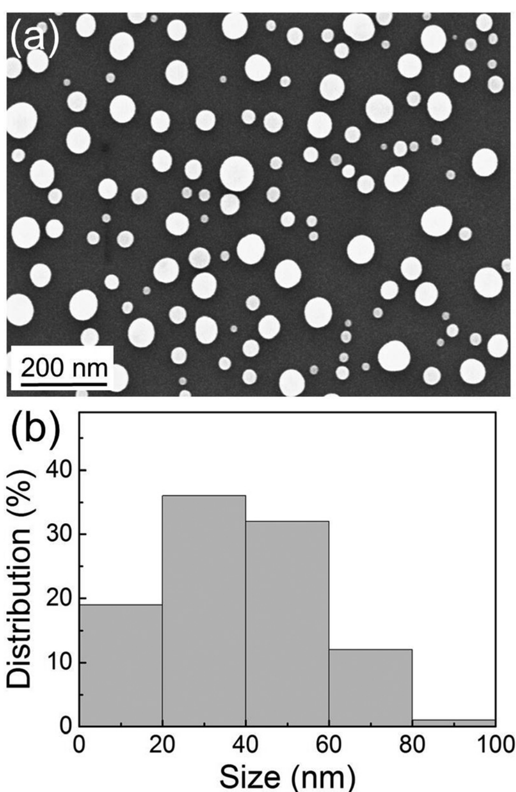

FIG. 2. (a) SEM plan-view of Ag nanoparticles after annealing the 10 nm Ag layer on top of semiconducting a-IZO channel material at 300 °C for 20 min in N_2 atmosphere; (b) Ag nanoparticle size distribution estimated from the plan-view SEM image.

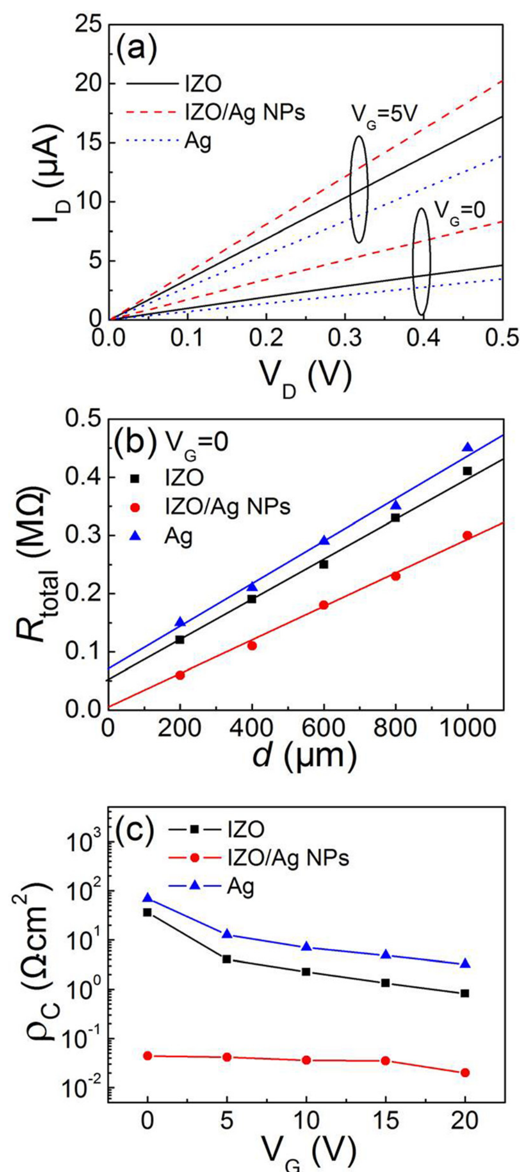

FIG. 4. (a) I_D-V_D curves at backgate bias $V_G = 0$ and 5 V in the $0 < V_D < 0.5$ V range; (b) total *R* vs. separation *d* plot from TLM patterned a-IZO TFTs at $V_G = 0$ bias; (c) specific contact resistance ρ_C as a function of $V_G = 0$–20 V in 5 V steps for the three types of contacts: conducting IZO; IZO with Ag NPs; and blanket Ag metal.

The TLM structures used in this work allow the evaluation of both specific contact resistance and, using the Si/SiO_2 back gate, TFT device performance. The analysis started with the measurement of I_D-V_D curves at backgate bias $V_G = 0$–20 V in 5 V steps in the $0 < V_D < 0.5$ V range for each of the three sets of devices: conducting-IZO/semiconducting-IZO, conducting-IZO/Ag-NPs/semiconducting-IZO, and 100-nm blanket Ag/semiconducting-IZO. As shown in Fig. 4(a), all the contacts show linear I_D-V_D curves at low V_D, indicating Ohmic contacts formed in all three structures for all V_G. Figure 4(b) shows a set of resistance R_{total} vs. electrode separation d plots for the three sets of devices at $V_G = 0$. The intercept and slope of each line were used to estimate contact resistance (R_C) and sheet resistance (R_S), respectively, using the relation

$$R_{total} = 2R_C + (R_S/W)d, \quad (1)$$

where $W = 2000\,\mu$m is the electrode width. For the three sets of samples, the specific contact resistance ρ_C was then determined from $R_C = (R_S\rho_C)^{1/2}/W$ and the results are summarized as a function of V_G in Fig. 4(c). We observe that for all V_G, the introduction of Ag NPs yields better contacts. In particular, at $V_G = 0$, where the carrier density n in the IZO channel is low, we find that conducting IZO contacts and planar Ag contacts have a high $\rho_C \sim 36$ and 68 $\Omega\,\text{cm}^2$, respectively, whereas contacts with Ag NPs at the homojunction interface exhibit a three orders of magnitude improvement in ρ_C to $4.4 \times 10^{-2}\,\Omega\,\text{cm}^2$. The carrier density n in the a-IZO channel is an important variable that affects contact resistance. However, the estimated n in the channel of each TFT obtained from the field effect mobility values μ extracted from the transfer characteristics in Fig. 5 via the relation $R_S \times t = (ne\mu)^{-1}$, where t is the channel thickness, is similar in the three sets of TFTs (at the same V_G). The TFT off current in each of the sets of devices is also similar which, again, suggests a similar channel n. As a result, the improved ρ_C in the devices with Ag NPs in the contacts is due to the NPs themselves, rather than changes in the a-IZO channel n or mobility μ.

To demonstrate the effect of using improved Ag NP-containing contacts on TFT performance, we measured the backgated output I_D-V_D transistor characteristics of $W/d = 2\,000/200\,\mu$m devices in a light-tight probe station by sweeping V_D from 0 to 30 V at gate voltage $V_G = -5$ to 20 V in 5 V steps. The results are shown in Figs. 5(a)–5(c) for the TLM-patterned a-IZO TFTs with the three types of contact metallization. All of the TFTs devices operate in depletion mode with an on-off ratio $>10^7$.

The corresponding transfer I_D-V_G characteristics in saturation, measured by sweeping V_G from -15 to 25 V at fixed $V_D = 30$ V, are shown in Figs. 5(d)–5(f). Under these conditions, the saturation current can be estimated as

$$I_D = \mu C_{ox}(W/d)(V_G - V_T)^2/2, \quad (2)$$

where $C_{ox} = 1.725 \times 10^{-8}$ F/cm^2 is the oxide capacitance, μ is the saturation field effect mobility, and V_T is the threshold voltage. The apparent μ can be derived from the slope of the $(I_D)^{1/2}$ *vs.* V_G curve, while V_T can be estimated by extrapolating the linear portion of the curve to zero drain current, see Figs. 5(d)–5(f). Since we have experimental access to the contact resistance R_C for all bias conditions, dashed lines in Figs. 5(d)–5(f) show the $(I_D)^{1/2}$ *vs.* V_G slope corrected for the contact resistance (the correction is insignificant for the TFTs with Ag NP-containing contacts, but does affect the mobility extraction for the other TFTs). We find that $\mu = 27 \pm 2\,\text{cm}^2/\text{V}\cdot\text{s}$ for all a-IZO channels, but that the improved contacts in Figs. 5(b) and 5(e) result in higher current and better on/off ratio compared to control samples without Ag NPs in at the contact junction.

These results indicate that improved TFT performance was realized by employing Ag NPs at the electrode-channel interface to decrease ρ_C. This is consistent with our previous work[14] that showed that high ρ_C results in the significant underestimation of the channel mobility.

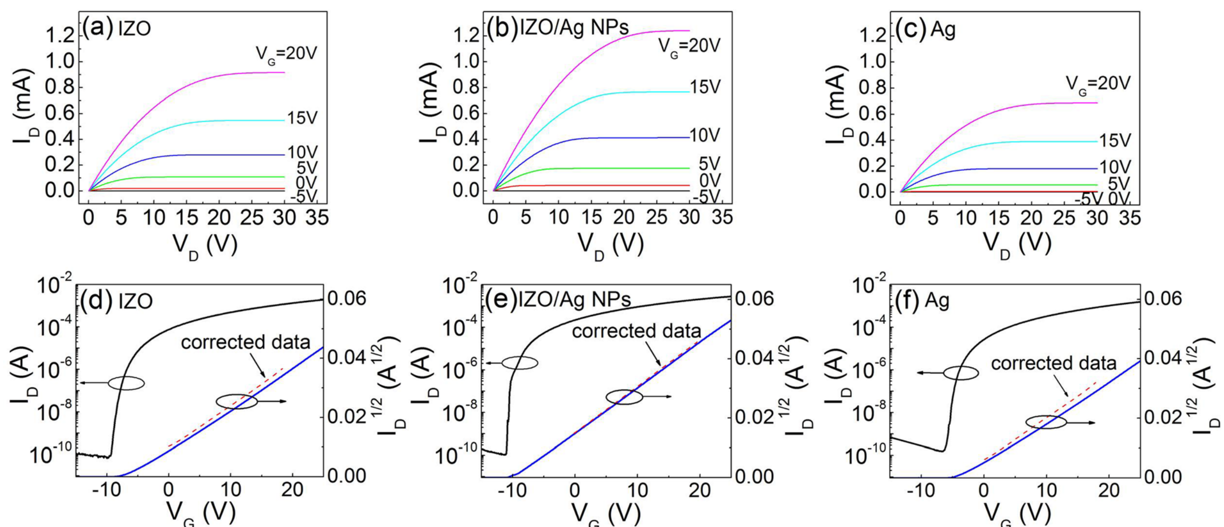

FIG. 5. Upper panels: output I_D-V_D characteristics vs. $V_G = -5$ to 20 V at 5 V intervals for (a) conducting IZO, (b) conducting-IZO/Ag NPs and (c) Ag electrodes. Lower panels: corresponding transfer I_D-V_G characteristics at $V_D = 30$ V, combined with $I_D^{1/2}$-V_G plots; dashed red lines represent data corrected for contact resistance. For all devices, $W/d = 2000/200\,\mu$m.

The physical mechanism for the lower ρ_C is the concentration of the electric field near the smaller ~10 nm Ag NPs.[15]

In summary, we have investigated the effect of placing Ag NPs at the compositionally homogeneous interface between a-IZO channel and IZO electrode on the specific contact resistance and its effect of the electrical performance of a-IZO TFTs. We have shown that Ag NPs decrease the specific contact resistance in homojunction a-IZO interfaces (by 3 orders of magnitude), leading to improved TFT performance. As a result, the formation of Ag NPs between channel and electrodes is a promising method to improve a-IZO TFT performance without a great penalty in fabrication complexity.

This work was supported by the National Science Foundation (DMR-1409590). Rui Xu acknowledges the financial support of the China Scholarship Council (CSC), whereas Jian He acknowledges the Fundamental Research Funds for the Central Universities (Grant No. ZYGX2012YB024) and the graduate student exchange program supported by the University of Electronic Science and Technology of China (UESTC).

[1] B. Yaglioglu, H. Y. Yeom, R. Beresford, and D. C. Paine, Appl. Phys. Lett. **89**, 062103 (2006).
[2] D. C. Paine, B. Yaglioglu, Z. Beiley, and S. Lee, Thin Solid Films **516**, 5894 (2008).
[3] J. I. Song, J. S. Park, H. Kim, Y. W. Heo, J. H. Lee, J. J. Kim, G. M. Kim, and B. D. Choi, Appl. Phys. Lett. **90**, 022106 (2007).
[4] P. Barquinha, G. Goncalves, L. Pereira, R. Martins, and E. Fortunato, Thin Solid Films **515**, 8450 (2007).
[5] Y. L. Wang, F. Ren, W. Lim, D. P. Norton, S. J. Pearton, I. I. Kravchenko, and J. M. Zavada, Appl. Phys. Lett. **90**, 232103 (2007).
[6] M. P. Taylor, D. W. Readey, M. V. Hest, C. W. Teplin, J. L. Alleman, M. S. Dabney, L. M. Gedvilas, B. M. Keyes, B. To, J. D. Perkins, and D. S. Ginley, Adv. Funct. Mater. **18**, 3169 (2008).
[7] R. Martins, P. Almeida, P. Barquinha, L. Pereira, A. Pimentel, I. Ferreira, and E. Fortunato, J. Non-Cryst. Solids **352**, 1471 (2006).
[8] S. Lee, H. Park, and D. C. Paine, J. Appl. Phys. **109**, 063702 (2011).
[9] P. C. Hsu, S. Wang, H. Wu, V. K. Narasimhan, D. Kong, H. R. Lee, and Y. Cui, Nat. Commun. **4**, 2522 (2013).
[10] B. Cho, J. Lee, H. Seo, and H. Jeon, Appl. Phys. Lett. **102**, 102108 (2013).
[11] D. Gupta, M. Anand, S. W. Ryu, Y. K. Choi, and S. Yoo, Appl. Phys. Lett. **93**, 224106 (2008).
[12] Z. Ma, M. Yan, X. Jiang, H. Yang, and G. Xia, Appl. Phys. Lett. **101**, 013106 (2012).
[13] S. Lee, K. Park, and D. C. Paine, J. Mater. Res. **27**, 2299 (2012).
[14] S. Lee, H. Park, and D. C. Paine, Thin Solid Films **520**, 3769 (2012).
[15] See, for example, J. D. Jackson, *Classical Electrodynamics*, 2nd ed. (Wiley, New York, 1975), pp. 75–78.